Fuel Effects on a Low-swirl Injector for Lean Premixed Gas Turbines

D. Littlejohn and R. K. Cheng

Environmental Energy Technologies Division
Lawrence Berkeley National Laboratory
Berkeley, CA 94720, USA

Corresponding Author:
David Littlejohn
Lawrence Berkeley National Laboratory
MS 70-108B, 1 Cyclotron Rd.
Berkeley, CA 94720
USA

Work: 1 510 486 7598
Fax: 1 510 486 7303
E-Mail: DLittlejohn@lbl.gov

COLLOQUIM 11. IC ENGINE AND GAS TURBINE COMBUSTION

SHORT TITLE: Fuel Effects on Low-swirl injector

KEYWORDS: gas turbines, lean premixed, swirl, NOx, alternate fuels

Word Count:	5810
Main Text (from MS Word)	**3250**
Equations (2 single line single column)	30
Tables	
Table 1 (M1)	134
Table 2 (M1)	218
Figures (including captions)	
Figure 1 (M1)	144
Figure 2 (M1)	216
Figure 3 (M1)	241
Figure 4 (M1)	136
Figure 5 (M1)	200
Figure 6 (M1)	220
Figure 7 (M1)	237
Figure 8 (M1)	279
Figure 9 (M1)	157
References (formula)	**349**

Abstract

Laboratory experiments have been conducted to investigate the fuel effects on the turbulent premixed flames produced by a gas turbine low-swirl injector (LSI). The lean-blow off limits and flame emissions for seven diluted and undiluted hydrocarbon and hydrogen fuels show that the LSI is capable of supporting stable flames that emit < 5 ppm NO_x (@ 15% O_2). Analysis of the velocity statistics shows that the non-reacting and reacting flowfields of the LSI exhibit similarity features. The turbulent flame speeds, S_T, for the hydrocarbon fuels are consistent with those of methane/air flames and correlate linearly with turbulence intensity. The similarity feature and linear S_T correlation provide further support of an analytical model that explains why the LSI flame position does not change with flow velocity. The results also show that the LSI does not need to undergo significant alteration to operate with the hydrocarbon fuels but needs further studies for adaptation to burn diluted H_2 fuels.

1. INTRODUCTION

Power generation turbines operating on natural gas are subjected to stringent emission rules and many urban areas have NO_x requirements of < 5 ppm (corrected to 15% O_2). Recent research has led to development of effective control technologies based on lean premixed combustion, such as catalytic combustors [1], trapped vortex combustors [2], and metal fiber combustors [3]. Our low-swirl injector (LSI) [4] provides another option that avoids altering engine layout or operating cycle. As more mid-size turbines are deployed in locations with readily available alternate fuels such as landfills, paper mills, and oil platforms, meeting emissions goals while using different fuels presents great challenges. This is due to differences in combustion properties and their interactions with turbulence that affect flame stability, emissions, and

2

turndown performance. Our goal is to investigate the fuel effects on turbulent premixed flames in the LSI to develop an engineering method to adapt it to operate on alternate fuels. The approach is to investigate lean blow-out (LBO), emissions and the flowfield characteristics to gain the fundamental insights for optimizing the LSI for fuel-flexibility.

2.   BACKGROUND

Lean premixed combustion is a proven dry-low-NO_x (DLN) method for natural gas-powered turbines. Most DLN engines emit NO_x < 25 ppm and CO < 50 ppm (both @ 15% O_2). But attaining ultra-low emissions of < 5 ppm NO_x requires that turbines operate at conditions close to the lean blowoff limit (LBO) where combustors are susceptible to combustion oscillations. In a previous paper [4] we reported the development of a LSI based on a low-swirl flame stabilization method that has been developed as a laboratory configuration for studying flame/turbulence interactions [5-8]. Results at turbine conditions ($500 < T_0 < 730$K, $6 < P_0 < 15$ atm, $12 < U_0 < 48$ m/s) show that the LSI produces stable flames with NO_x and CO below 2 ppm (@15% O_2) at the leanest conditions. Further work has led to a second LSI that has been evaluated in a single cylindrical combustor and in a multi-injector annular combustor at simulated engine conditions [9]. The study showed that the LSI has good performance characteristics, and is stable over a wide range of conditions where NO_x < 5 ppm and CO well below the acceptable limit of 400 ppm. The flame does not have a propensity to become unstable towards blowoff or show undesirable injector-to-injector interaction. Testing of this LSI prototype in a 7 MW gas turbine is scheduled in 2006.

The heart of the LSI is a swirler evolved from atmospheric low-swirl burners [10]. The swirler section is 2.8 cm long (L_s), and has an outer radius of 3.17 cm (Fig. 1) and sixteen curved vanes

(vane angle $\alpha = 42°$ at the exit) attached to the outer surface of a $R_c = 2$ cm centerchannel. The open centerchannel allows a portion of reactants to remain unswirled and this nonswirling flow inhibits flow recirculation and promotes formation a divergent flowfield, a key feature of the flame stabilization mechanism [8]. To control the mass ratio, $m = {m_c}/{m_s}$, between the flows through the centerchannel, m_c, and the swirled annulus, m_s, a perforated screen is fitted at the entrance of the centerchannel (Fig. 1 right). From Ref [4, 11] the swirl number definition is:

$$S = \frac{2}{3}\tan\alpha \frac{1-R^3}{1-R^2+m^2\left({1}/{R^2}-1\right)^2 R^2} \qquad \text{Eq. 1}$$

Here the ratio of the radii of the centerchannel and injector, R, is 0.63 and the screen blockage controls m and hence S. The LSI for this study is slightly different than an earlier version [4] in that it uses the swirler for the second prototype. Fitted with a 58% blockage screen, this LSI has $S = 0.57$ compared to $S = 0.5$ from the earlier study. Otherwise, all dimensions e.g. exit tube length of $l_i = 9.5$ cm and a 45° tapered edge, remain unchanged.

3. EXPERIMENTAL SYSTEM AND DIAGNOSTICS

For the lean blowout (LBO) and Particle Image Velocimetry (PIV) investigations, the LSI was mounted on a cylindrical settling chamber. Air (up to 1800 LPM) enters at the side of a 25.4 cm diameter chamber and flows into the LSI via a centrally placed 30 cm long straight tube. Air flow is adjusted by a valve and monitored by a turbine meter, and fuel (Table I) is injected in the air supply to ensure a homogeneous mixture for the injector. Both the fuel and the PIV seeder flows are controlled by mass flow controllers and set according to a predetermined value of ϕ with a PC.

The fuels listed in Table I consist of hydrocarbons, N_2 and CO_2-diluted CH_4 to simulate landfill and biomass fuels, H_2-enriched CH_4 to simulate refinery gas and CO_2-diluted H_2. Variations in the combustion properties are shown in Table I by the stoichiometric adiabatic flame temperatures, T_{ad}, and laminar flame speeds, S_L. For the blended fuels, these properties were calculated using an algorithm by Zhang et al. [12]. The Wobbe Index is used commercially as an indicator of fuel interchangeability and the range of values (Table I) for our fuels are equivalent to those from landfill gas to liquified petroleum gas.

Emission measurements were performed with a Horiba PG-250 analyzer, calibrated using 7.9 ppm NO in N_2 and 31.8 ppm CO in N_2 (Scott Specialty Gases). The instrument has an accuracy of $\pm$ 0.5 ppm for NO_x. To measure emissions, flames were enclosed in a 16 cm diameter, 20 cm high quartz tube and sampled with a probe place a few cm above the center of the tube. This arrangement is similar to the atmospheric rig used previously [4]. The collected exhaust gas was cooled and water was removed with a dessicant before it flowed into the analyzer.

To facilitate PIV data collection, the non-reacting flows and the flames were not enclosed. Details of the PIV system and data analysis are described in [4]. It has a New Wave Solo PIV laser with double 120 mJ pulses at 532 nm and a Kodak/Red Lake ES 4.0 digital camera with 2048 by 2048 pixel resolution. The optics were configured to capture a field of view of 13 cm by 13 cm. A cyclone particle seeder seeds the air flow with 0.3 μm Al_2O_3 particles. Data analysis was performed on the 224 image pairs recorded for each experiment using software developed by Wernet [13]. Using 64x64 pixels cross-correlation interrogation regions with 50% overlap, this rendered a spatial resolution of approximately 2 mm.

4. RESULTS

4.1. Flame Stability and Lean Blowoff

Flame stability and LBO were determined at volumetric flow rates $300 < Q < 1880$ LPM, corresponding to bulk flow velocities of $3 < U_0 < 9$ m/s. Fig. 2(a) shows LBO data for methane. The open flame data at STP [4] are shown as the baseline. The data at higher inlet temperatures and pressures (1 to 14 atm, 620-770 K) were obtained from enclosed configurations simulating a gas turbine combustor and they show the lowest LBO occur at heated atmospheric tests in a quartz rig [4]. These data also show that the LSI can operate up to $U_0 = 85$ m/s, and that LBO remains relatively insensitive to U_0. This is a desirable feature for turbines for it indicates that the LBO will not edge closer to the operating point of the combustor when the load increases. In Fig 2(b) LBO values are essentially the same for CH_4, C_3H_8, 0.5 CH_4/0.5 CO_2, and 0.6 CH_4/0.4 N_2. The dilution of CH_4 by inerts has no observable effect on LBO. LBO is slightly lower for C_2H_4 and 0.6 CH_4/0.4 H_2, which have higher flame speeds than the other fuels. The LBO values for H_2 are very low and do not show a significant effect due to dilution. However, the stability ranges for H_2 fuels are limited because the flames tend to reattach to the burner rim at $\phi > 0.30$.

NO_x and CO emissions from flames at $Q = 1500$ LPM ($U_0 = 7$ m/s) are shown in Figure 3. Only data for the hydrocarbon fuels are plotted as emissions from H_2 fuels were below detectable limits. For the hydrocarbon fuels, NO_x has an exponential dependence on ϕ, and at a given ϕ, emissions show a dependence on Wobbe Index, consistent with the higher heat content of these fuels. However, the significant implication of these data is that regardless of fuel content the LSI supports stable flames emitting < 5 ppm NOx and the conditions are well above the LBO point.

As suggested by Figure 3, flame temperature is an important parameter in NO_x formation in the LSI. The plot of NO_x vs. T_{ad} in Figure 4 shows that NO_x correlates well with T_{ad} and is

consistent with data at high T_0, P_0 and U_0 [4]. As discussed previously, the LSI flow has little or no recirculation, which may explain why the NO_x production depends primarily on flame temperature.

4.2. Flowfield Analysis

Table II shows the PIV experimental conditions consisting of three non-reacting flows and sixteen flames. For hydrocarbon flames, their stoichiometries were set at the conditions where $NO_x \approx 5$ ppm to compare them at the conditions that meet the emission goals. For the diluted hydrogen fuels, flames at $\phi = 0.25$ and 0.30 were studied.

The centerline profiles for three non-reacting flows are compared in Figure 5. The similarity feature of the flowfields is shown by the normalized U/U_0 profiles of Figure 5(a) collapsing onto a consistent trend. In a previous paper, [14] two parameters were introduced to characterize the nearfield region. The first is the virtual origin, x_0, of the divergent flow, obtained by extrapolating the linear velocity decay region downstream of the exit (Fig 5(a)), and second is the slope of the linear extrapolation that quantifies the normalized axial divergence rate, $a_x = dU/dx/U_0$. Values of x_0 and a_x for the three flows are given in Table II and they are very close. Profiles of the normalized 2D turbulent kinetic energy, $q' = ((u'^2 + v'^2)^{1/2})/2$ of Fig 5(b) show that within the linear velocity decay region, turbulence along the centerline remains constant. But the 2:1 ratio between u' and v' indicates that it is anisotropic. These characteristics can be attributed to the effect of annulus swirling flow. In the farfield, slight increases in q'/U_0 at x > 60 mm are consistent with the formation of a very weak recirculating zone [4].

Radial profiles of the non-reacting flows at x = 15 mm are shown in Fig 6, where they all exhibit similarity behavior. In Fig 6(a), the U/U_0 profiles have a flat central region corresponding to the

centerchannel non-swirling flow flanked by two velocity peaks, corresponding to the swirling flow. In Fig 6(b), linear distribution of the V/U_0 profiles within the center region ($-15 < r < 15$ mm) show that the normalized radial divergence rates $a_r = dV/dx/U_0$ are about half that of a_x. Therefore, the overall features of the nearfield are consistent with those of other divergent flows (e.g. stagnating flows). The q'/U_0 profiles (Fig 6(c)) have relatively flat distributions in the center regions surrounded by intense turbulence peaks. The shear stresses (not shown) at the center regions are very low ($\overline{uv} \approx 0.005$ m/s) and increase to very high levels ($\overline{uv} \approx 1.5$ m/s) towards the swirling regions. These velocity statistics show that the LSI produces a uniform central region with low shear stresses for flame stabilization.

Centerline profiles for reacting flows are compared in Figure 7. Only the eight flames with $9.3 < U_0 < 9.6$ m/s are shown for clarity. Despite the large difference in the farfield, all U/U_0 of Fig 7 (a) have linear velocity decays near the LSI exit. The positions where profiles deviate from linear decay trends correspond to the leading edges of the turbulent flame zones. From these centerline profiles, a_x and x_0 for the nearfield linear decay regions can be deduced. Results listed in Table II show that the flames increase both a_x and x_0 to demonstrate an influence of the flame on mean characteristics of the upstream reactant flow. For hydrocarbon flames, the majority of the a_x values are around -0.014 mm^{-1} compared to $a_x = -0.085$ mm^{-1} for the non-reacting flows. For the diluted H_2 flames, the increases in a_x are smaller, averaging -0.011 mm^{-1} and their U/U_0 profiles have different shapes than the hydrocarbon flames. This seems to be associated with the lower heat release compared to the hydrocarbon flames. Though the hydrocarbon flame profiles are consistent in the nearfield, their farfield features show dependence on heat release. Significant flow accelerations are found only in the C_2H_4 and 0.5 $CH_4/0.5$ H_2 flames, while other hydrocarbon flame profiles have relatively flat distribution. The corresponding q'/U_0 profiles of

8

Fig 7(b) show that the fluctuation levels at the LSI exit are slightly higher than in the non-reacting flows. But the anisotropic ratio u':v' remains unchanged. The q'/U_0 levels remain relatively flat through the flame brushes and the increases in the farfield at x > 80 mm corresponds to flames that produce weak recirculation.

Figure 8 shows radial profiles at x = 15 mm for flames of Fig 7. These positions are below the flame brushes so that the results can be compared with those of Fig 6. Although the U/U_0 profiles in Fig 8(a) and Fig 6(a) have similar features, there are quantitative differences. Within the central flat regions, U/U_0 levels decrease to 0.5 for the two diluted H_2 flames, and 0.3 for hydrocarbon flames. These changes correspond to increases in a_x and x_0. The center regions are also slightly wider than in the non-reacting flows. Another difference is peak velocity in the surrounding swirl annulus increasing from $U/U_0 = 1.2$ in non-reacting flows to 1.5 in the flames.

The v/U_0 profiles of Fig 8(b) all collapse onto a consistent distribution, giving further evidence for flow similarity in the divergent flow regions upstream of the flames. The slopes of the center region are also larger, but the 2:1 ratio between a_x and a_r is preserved. Another observable effect of the flame is that the minimum and maximum V/U_0 values corresponding to the U/U_0 peaks also increase to show higher radial outflow. In Fig 8(c), the q'/U_o levels in the center region are more scattered due to the influence of flames but the overall shape remain the same as in Fig 6(c).

Our flowfield analysis indicates that the overall effect of the flame is that of an aerodynamic blockage against the flow out of the LSI. The net effects are a systematic shift of the divergence flow into the LSI, increases in the divergence rates, and increases in U and V in the swirl

regions. These effects are weaker for flames with low heat releases. Despite these systematic changes, the similarity features of the center region are preserved.

4.3. Turbulent Flame Speed

The turbulent flame speed, S_T is the basic turbulent flame property that explains the LSI stabilization mechanism because the freely propagating flame settles at the point within the center divergent flow region where the mean flow velocity is equal and opposite to S_T. Although the definition of S_T, its linear or non-linear dependence on u' [15] and also its theoretical significance [16] have been subject of much debate, the fact that the LSI supports stable flames from $3 < U_0 < 85$ m/s indicates that the S_T deduced from the LSI has practical engineering significance, and provides necessary insight for further development. From previous studies using LSBs with air-jets [17, 18], it has been shown that S_T/S_L correlates linearly with u'/S_L. More recent data from the CH_4/air LSI flames at $7 < U_0 < 22$ m/s [14] and from two 5.08 cm ID LSBs of R = 0.8 and 0.6 [10] give further support to this correlation.

The S_T deduced from the current data are listed in Table II. Here, as in [14], S_T is defined by the velocity at the point where the centerline U_0 profile deviates from its initial linear decay. The effects of fuel composition on S_T are shown by their values listed in Table II. Despite the low heat release rates, the S_T of the diluted H_2 flames are higher than the S_T of the hydrocarbon flames. In Table II, only the u'/S_T and S_T/S_L for the hydrocarbon flames are listed because reliable S_L data for very lean diluted H_2 mixtures are not available. From Fig. 9 it can be seen that the S_T of the hydrocarbon flames are consistent with previous results [14, 18] where they are well within the experimental scatter. The inclusion of the twelve hydrocarbon flames did not affect the correlation of $S_T/S_L = 1 + 2.16$ u'/S_L. Although the S_T for diluted H_2 cannot be

compared directly with hydrocarbon flame data, the fact that their S_T are higher strongly suggests that their turbulent flame speeds will not be consistent with those in Fig. 9.

5. DISCUSSION

Ref. [14] reports that the similarity features of divergent flow in the nearfield coupled with a linear correlation of S_T give an explanation on why the flame remains stationary regardless of U_0. This stems from a balanced equation at the leading edge of the flame brush, x_f,

$$1 - \frac{dU}{dx}\frac{(x_f - x_o)}{U_o} = \frac{S_T}{U_0} = \frac{S_L}{U_0} + \frac{2.16u'}{U_o} \qquad \text{Eq. 2}$$

On the LHS, $dU/dx/U_o$ is the normalized axial divergence rate a_x. As shown in Table II, the values for the hydrocarbon flames are about -0.014 (mm^{-1}). On the far RHS, contributions from S_L/U_0 become small for large U_0 because S_L for lean flames are typically from 0.1-1.5 m/s. The second term on the RHS is dominant and is constant because u'/U_0 is controlled by the perforated plate. Consequently, $x_f - x_0$ does not vary significantly for large U_0.

Ref. [14] indicates that a practical application of Eq. 2 is to predict flashback velocity for natural gas flames. Also, with improved knowledge of S_T correlation and coupling of the nearfield divergence flow structures with combustion heat release, it can be the basis for developing guidelines to adapt the LSI for different fuels. Since the hydrocarbon flames have the same effect as CH_4 flames on a_x and x_0 and have the same S_T correlation, significant adjustments may be unnecessary for the current LSI to utilize hydrocarbon fuels with higher and lower Wobbe indices. Of course, this conjecture must be verified by higher velocity tests at elevated T_0 and P_0. As to the highly lifted diluted hydrogen flames, experience indicates that they will eventually become unstable at higher U_0. To improve stability, they need to be drawn closer to the exit. Eq.

2 shows that a larger a_x would be necessary and this can be accomplished by increasing S. As flame speed correlations for the H_2 fuels are likely to be different, Eq. 2 offers a means to estimate how flame positions changes with a_x and different S_T correlation.

6. CONCLUSIONS

Laboratory experiments have been performed to investigate the fuel effects on a low-swirl injector developed for natural gas turbines. The experimental fuels comprise a typical range (characterized by the Wobbe indices of 1430 to 17800 kcal/Nm^3) for on-site power generation.

The LBO experiments show that the LSI with S = 0.57 supports stable flames for all seven fuels. The stability range for 0.5 H_2/0.5 CO_2 flames is limited to $\phi < 0.3$ where NO_x emissions are below detectible limits. NO_x emissions from the hydrocarbon flames show an exponential dependence on ϕ and correlate with T_{ad} and are consistent with previous measurements at $500 < T_0 < 700$ K and $6 < P_0 < 15$ atm. Despite the variations in fuel properties, the LSI is capable of supporting stable hydrocarbon flames that emit $NO_x < 5$ ppm and CO well below acceptable limits.

Analyses of the non-reacting and reacting flowfields indicate that the overall effect of the flame is that of an aerodynamic blockage against the flow supplied through the LSI. The net result is a systematic shift of the divergence flow into the LSI, increases in the divergence rates and increases in the mean axial and radial velocities in the swirl annulus region. These effects are weaker for the flames with lower heat releases. However, the virtual origin of the flow divergence, x_0, and its non-dimensional stretch rates a_x show that the similarity features of the nearfield region are preserved. The turbulent flame speeds, S_T, of the hydrocarbon fuels are consistent with those of methane/air flames. The similarity features and linear S_T correlation

provide further support of an analytical model that explains why the lifted LSI flame does not shift with U_0.

This study shows that the LSI does not need to undergo significant alterations to operate with the hydrocarbon fuels, but need further studies for adaptation to burn diluted H_2 fuels.

7. ACKNOWLEDGEMENT

8. REFERENCES

[1]   R. Carroni, V. Schmidt and T. Griffin, Catalysis Today, 75 (1-4) (2002) 287-295.

[2]   V. R. Katta and W. M. Roquemore, Journal of Propulsion and Power, 14 (3) (1998) 273-281.

[3]   S. J. Greenberg, N. K. McDougald, C. K. Weakley, R. M. Kendall and L. O. Arellano, Journal of Engineering for Gas Turbines and Power-Transactions of the ASME, 127 (2) (2005) 276-285.

[4]   M. R. Johnson, D. Littlejohn, W. A. Nazeer, K. O. Smith and R. K. Cheng, Proc. Comb. Inst, 30 (2005) 2867 - 2874.

[5]   I. G. Shepherd, R. K. Cheng, T. Plessing, C. Kortschik and N. Peters, Proc. Comb. Institute, 29 (2002) 1833 - 1840.

[6]   R. K. Cheng, D. A. Schmidt, L. Arellano and K. O. Smith, IJPGC2001, New Orleans, 2001

[7]   D. T. Yegian and R. K. Cheng, Combustion Science and Technology, 139 (1-6) (1998) 207-227.

[8]   C. K. Chan, K. S. Lau, W. K. Chin and R. K. Cheng, Proc. Comb. Inst., 24 (1992) 511-518.

[9]   W. A. Nazeer, K. O. Smith, P. Sheppard, R. K. Cheng and D. Littlejohn, ASME Turbo Expo 2006: Power for Land, Sea and Air, Paper GT2006-90150 ASME, Barcelona, Spain, 2006,

[10]   R. K. Cheng, D. T. Yegian, M. M. Miyasato, G. S. Samuelsen, R. Pellizzari, P. Loftus and C. Benson, Proc. Comb. Inst., 28 ((2000) 1305-1313.

[11]   D. Littlejohn, M. J. Majeski, S. Tonse, C. Castaldini and R. K. Cheng, Proc. Comb. Inst., 29 ((2002) 1115 - 1121.

[12]   Q. Zhang, D. R. Noble, A. Meyers, K. Xu and T. Lieuwen, ASME Turbo Expo 2005: Power for Land Sea and Air, Paper GT2005-68907 Reno, NV, 2005.

[13]   M. P. Wernet, 18th International Congress on Instrumentation for Aerospace Simulation Facilities, Toulouse, France, 1999,

[14]   R. K. Cheng, D. Littlejohn, W. A. Nazeer and K. O. Smith, ASME Turbo Expo 2006: Power for Land Sea and Air, Paper GT2006-90878 ASME, Barsalona, Spain, 2006.

[15]   D. Bradley, Proc. Comb. Inst., 24 (1992) 279-285.

[16]   T. Plessing, C. Kortschik, M. S. Mansour, N. Peters and R. K. Cheng, Proc. Comb. Inst., 28 (2000) 359-366.

[17]   R. K. Cheng, I. G. Shepherd, B. Bedat and L. Talbot, Combustion Science and Technology, 174 (1) (2002) 29-59.

[18]   B. Bedat and R. K. Cheng, Combustion and Flame, 100 (3) (1995) 485-494.

TABLES

Table I

Fuel Composition	T_{ad} at $\phi = 1$ K	S_L at $\phi = 1$ m/s	Wobbe Index kcal/Nm^3
CH_4	2230	0.39	11542
C_2H_4	2373	0.74	14344
C_3H_8	2253	0.45	17814
H_2	2318	2.50	9712
0.5 CH_4/ 0.5 CO_2	2013	0.20	4182
0.6 CH_4/ 0.4 N_2	2133	0.31	6026
0.6 CH_4/ 0.4 H_2	2258	0.57	10130
0.5 H_2/ 0.5 CO_2	1693	0.56	1432

Table II

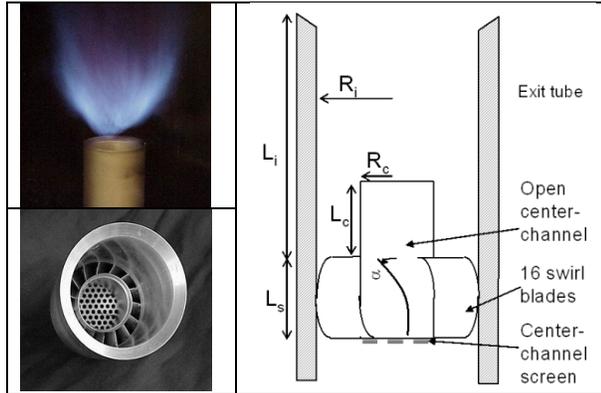| Fuel	ϕ	U_0 m/s	a_x mm^{-1}	x_0 mm	S_T m/s	u'/s_L	S_T/s_L
None	0	6.76	-0.0086	-21.41			
		7.47	-0.0085	-23.45			
		9.21	-0.0082	-24.62			
CH_4	0.73	6.23	-0.0141	-38.93	1.40	2.43	6.03
		9.27	-0.0134	-38.81	1.97	2.99	8.49
C_2H_4	0.62	6.32	-0.0140	-33.57	1.62	2.30	6.23
		9.40	-0.0130	-45.88	2.17	3.00	8.35
C_3H_8	0.69	6.23	-0.0131	-40.92	0.92	1.80	3.67
		9.30	-0.0134	-42.84	1.20	2.24	4.80
0.5 CH_4/ 0.5 CO_2	0.83	6.27	-0.0131	-42.10	1.00	3.18	7.11
		9.50	-0.0154	-38.70	1.46	4.51	10.43
0.6 CH_4 / 0.4 N_2	0.76	6.24	-0.0142	-38.94	1.16	2.45	6.44
		9.40	-0.0142	-42.75	1.56	3.69	8.67
0.6 CH_4/ 0.4 H_2	0.65	6.58	-0.0108	-55.95	1.43	2.14	6.50
		9.13	-0.0120	-45.08	2.24	2.91	10.18
0.5 H_2/ 0.5 CO_2	0.25	6.48	-0.0121	-32.89	1.42		
		9.55	-0.0102	-34.08	2.91		
	0.3	6.56	-0.0110	-27.27	2.54		
		9.38	-0.0094	-33.70	4.00		

FIGURE CAPTIONS

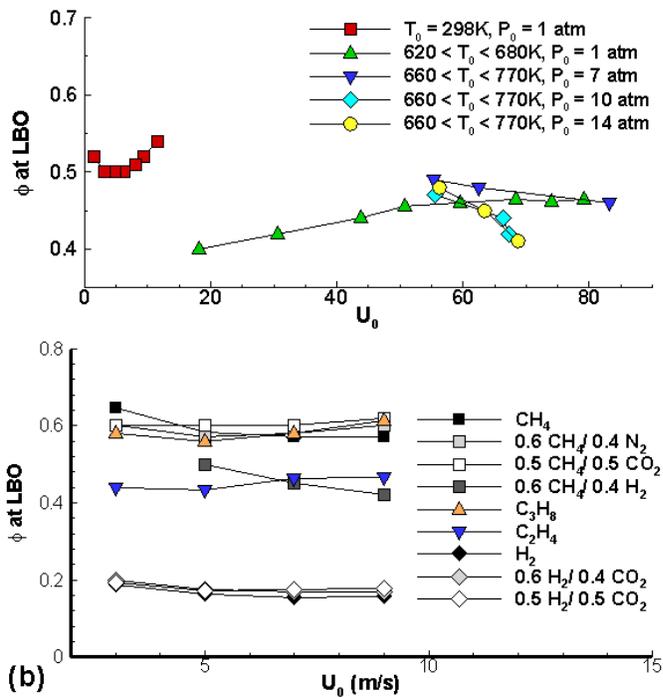Figure 1. Schematics and photographs of the low-swirl injector

Figure 2. LSI lean blow-off limits for (a) natural gas at STP and elevated T_0 and P_0 and for (b) fuels of Table I at STP
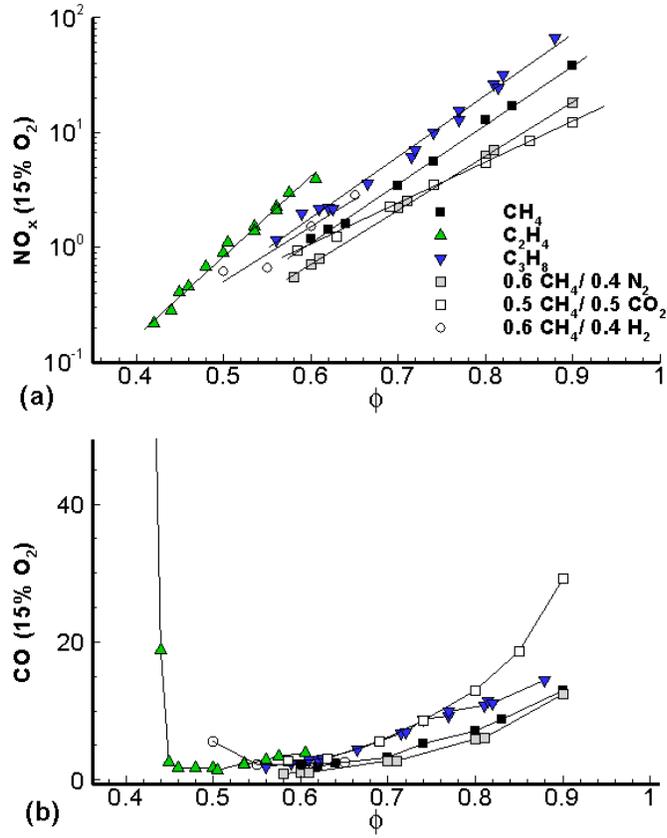
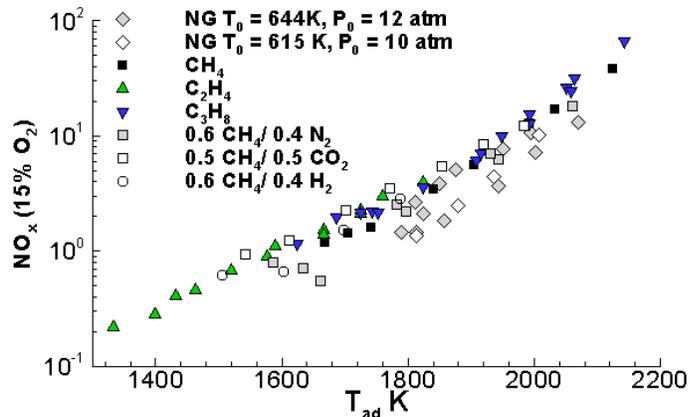Figure 3. NO_x and CO emissions from LSI for the hydrocarbon fuels of Table I

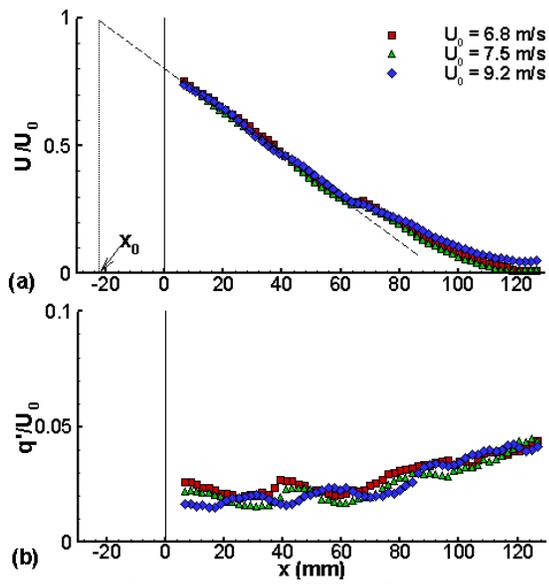Figure 4. Comparison of NO_x data from Figure 3 and from Ref [4].

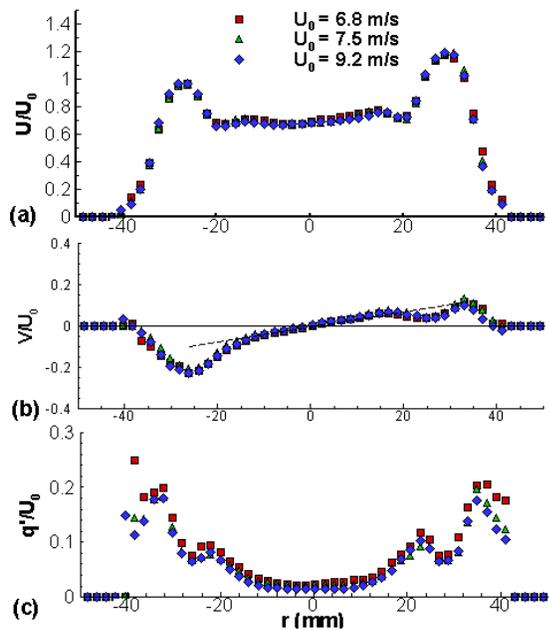Figure 5. Centerline profiles of the non-reacting flows

Figure 6. Radial profiles of the non-reacting flows at x = 15 mm

Figure 7. Centerline profiles of eight flames with $9.2 < U_0 < 9.5$ m/s

Figure 8. Radial profiles of eight flames with $9.2 < U_0 < 9.5$ m/s at x = 15 mm

Figure 9. Correlation of flame speeds measured from LSI and LSB

Figure 1 Schematics and photographs of the low-swirl injector

Figure 2 LSI lean blow-off limits for (a) natural gas at STP and elevated T_0 and P_0 and (b) for fuels of Table I at STP

Figure 3 NO$_x$ and CO emissions from LSI for the hydrocarbon fuels of Table I

Figure 4 Comparison of NO$_x$ data from Figure 3 and from Ref [4].

Figure 5 Centerline profiles of the non-reacting flows

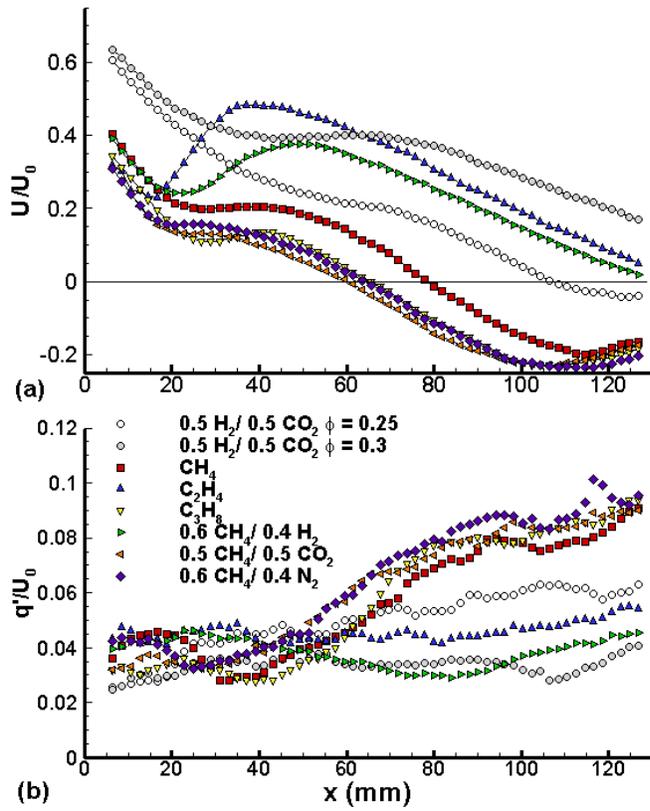Figure 6 Radial profiles of the non-reacting flows at x = 15 mm

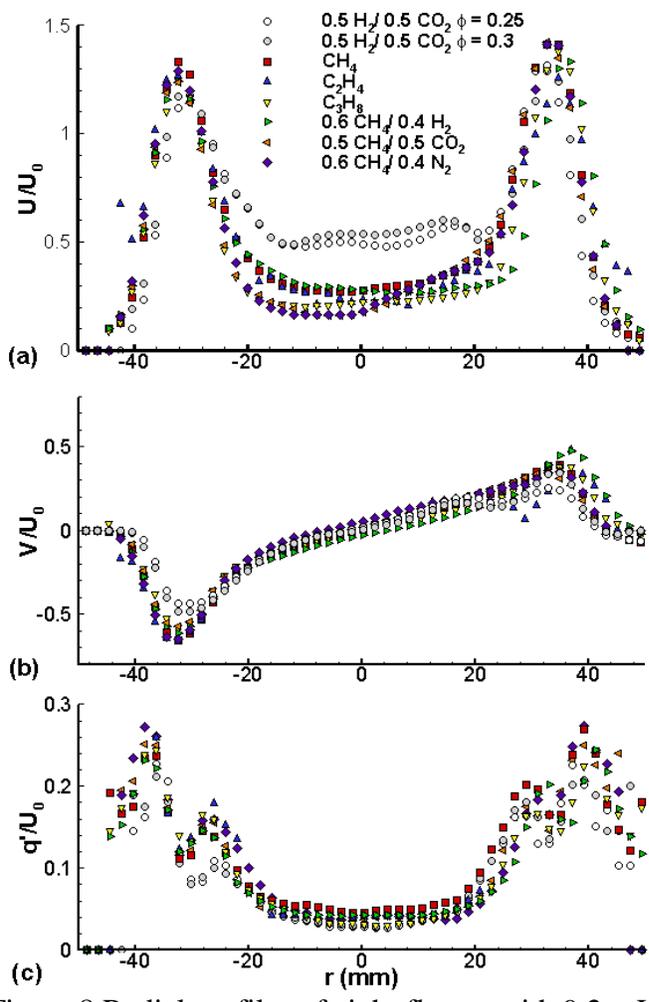Figure 7 Centerline profiles of eight flames with $9.2 < U_0 < 9.5$ m/s

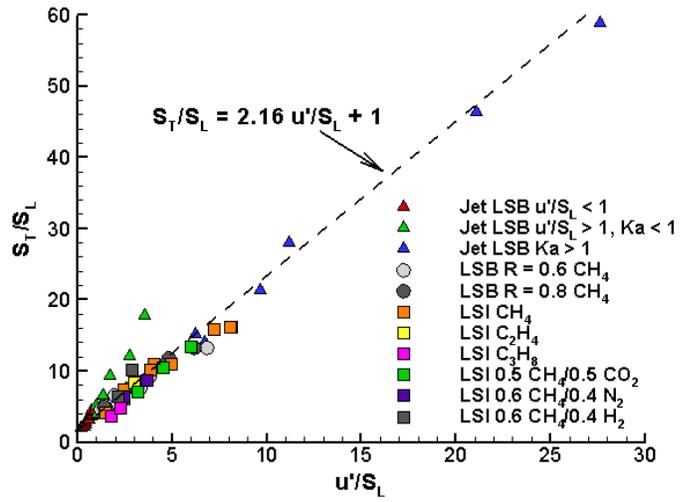Figure 8 Radial profiles of eight flames with $9.2 < U_0 < 9.5$ m/s at $x = 15$ mm

Figure 9 Correlation of flame speeds measured from LSI and LSB